IRANIAN JOURNAL OF PHYSICS RESEARCH

Iranian Journal of Physics Research, Vol. 18, No. 3, 2018

Carbon K edge structures of molecular crystals from first-principles: A comparison between phenanthrene and anthracene

H Nejatipour and M Dadsetani
Department of Physics, Lorestan University, Khoramabad, Iran

E-mail: dadsetani.m@lu.ac.ir

(Received 05 November 2016 ; in final form 06 September 2017)

Abstract
By means of ab-initio calculations on the basis of the FPLAPW method, we compared the energy loss near edge structure (ELNES) of carbon K edges in crystalline phenanthrene and its isomer, anthracene. In these two organic compounds, different non-equivalent carbon atoms can result in distinct K edge spectra due to the different carbon-carbon bond lengths, as a characteristic behavior of the molecular crystals. The smaller bond lengths push the ELNES features to the higher energies. In anthracene, the energy position of the edge-onset appears at lower energies due to its smaller electronic band gap. At the onset of the C K edge of anthracene, the strong splitting of the π^* peak into two peaks is observable. Compared to the C K edge in anthracene, due to the slightly larger C–C bond length in phenanthrene, the peak position of the main σ structure has a red shift. The ELNES spectrum of crystalline phenanthrene includes electron transition of 1s carbon orbital to π^* and σ^* states. In anthracene, the first two intense features have contributions of π^* orbitals. Consideration of the core-hole approximation by means of super-cells and the collection of semi-angles at magic value are essential to obtain reasonable ELNES spectra.

Keywords: organic molecular crystals, phenanthrene, anthracene, ELNES, density functional theory

1. Introduction

In recent years, the investigation of physical properties of organic solids has received much attention [1, 2]. Their wide variety and interesting physical properties give rise to organic solids that have a great potential for applying in electronic and opto-electronic devices such as organic light emitting diodes, photovoltaic cells and organic thin-film field-effect transistors [3-6]. Aromatic molecular crystals made of the small organic molecules are an attractive subclass of organic solids. They are composed of the continuous joint benzene rings in the linear or angular geometries. These organic semiconductors and their derivatives have been the focus of many researches in the field of electronics and photonics [7-10]. The high charge carrier mobility and the small band gaps ensure that molecular crystals can be suitable candidates for electronic and photovoltaic devices [11-13]. Oligoacenes (linear geometry) and phenacenes (angular geometry) are the isomer semiconducting aromatic hydrocarbons with the large and delocalized π–electron networks. Anthracene and phenanthrene formed of three joint benzene rings have the same molecular formula $C_{14}H_{10}$; the former belongs to the oligoacenes and the latter to the phenacens classes. Anthracene, a well-known oligoacene, has been the focus a wide variety of experimental and theoretical solid state studies, whereas its isomer, phenanthrene, has been less considered as a case under solid state investigations. For example, the effect of the inter-molecular interactions on structural, electronic, and optical properties of anthracene under hydrostatic pressure has been reported [14, 15]. Experimental and theoretical studies on phenanthrene are limited to determine the optical band gap [16] and superconductivity originating from the potassium and lanthanum doping [17]. In addition, pretty recently, we have studied the electronic structure and optical properties of phenanthrene and its phase under pressure in the framework of both RPA approximation and many-body perturbation theory, focusing on the electron-hole interaction and excitonic effects in the band gap region [18, 19]. The structural similarities of phenanthrene and anthracene hydrocarbons encourages researchers to compare and understand their electronic behavior.

For electronic applications determining the performance of the electronic and opto-electronic devices, the identity of the electronic properties plays a crucial role. Hence, the detailed understanding of the

electronic structure is a prerequisite for electronic applications of anthracene and phenanthrene. Moreover, the reliable procedures for recognizing the electronic properties can be achieved from the spectroscopic methods. Energy loss near edge structure (ELNES) is an important core level spectroscopy technique for understanding the structural, chemical and electronic information of different classes of materials. ELNES measures the energy loss of a high-energy electron beam scattered through a sample in the electron microscopes [20]. Since ELNES corresponds to the inelastic losses from the excitation of an electron from a core level into unoccupied states up to about 50 eV above the threshold in the system, such core loss traces straightly reflect the electronic structure of the excited unoccupied electron states. The probed transitions from core levels into empty or partially filled electronic states are element specific and very sensitive to the local bonding environment and coordination [21, 22].

However, the quantitative experimental dissections for interpreting near edge spectra are not present. This causes thatthe ab-initio calculations to become the superior tools to analyze the experimental spectra. There are various available theoretical approaches and computer codes based on different methods to calculate the ELNES spectra by means of the electronic structure calculations. One commonly used method is based on the density functional theory (DFT) code WIEN2k [23]. In the framework of the band structure methods, ELNES spectra of the bulk materials efficiently are calculated in WIEN2k. Some approximations have led to the extreme analogy among WIEN2k calculations and the experimental spectra [24]. The widespread ELNES studies, particularly carbon based materials, by means of the WIEN2k confirm these statements [25-27].

There are some experimental and theoretical fine structure reports for both molecular and crystalline phenanthrene and anthracene. By means of NEXAFS analysis, Klues *et al*. measured fine structure of molecular anthracene [28]. They have provided a detailed discussion about the K edges of some non-equivalent carbon atoms in anthracene. Gordon *et al*. have also studied the inner-shell excitation spectra of some aromatic compounds like benzene, naphthalene, anthracene, phenanthrene, triphenylene, pyrene, and 1, 2-benzanthracene in gaseous and molecular phases [29]. By symmetry characters, they have explained a difference in the general trend of naphthalene and anthracene, having significant π^* intensity spread over a larger energy range relative to phenanthrene and 1, 2-benzanthracene. Focused on the effect of po tassium doping, Pitman *et al*. have theoretically and experimentally studied conductivity in anthracene and phenanthrene by means of X-ray absorption spectroscopy (XAS) [30]. Although the effect of core-hole left by the electron transition is important and it may redistribute the oscillator strength in the whole ELNES spectra, Pitman *et al*. have not taken computational spectra into account .

ELNES measures the distribution of inelastically scattered electrons as a function of both energy loss and scattering angle. Since ELNES originates from electron transition to the unoccupied states, its results can be a complete description of the density of states (DOS) above the Fermi level, atomic arrangements, electronic structures and the chemical bonding of an objective atom in the materials. These transitions are element specific and very sensitive to the local bonding environment and coordination. They focus on ionization edges in the core loss region, and its advantage over X-ray absorption near edge structure (XANES) is its efficiency in the study of the electronic structure on the atomic scale, since only electrons can probe matter on the nanoscale. ELNES and XANES are based on the excitation of core electrons. XANES is usually performed on the bulk samples, because the cross section for the interaction of X-rays is much smaller than that of electrons. XANES cannot easily provide spatially resolved information due to the problems of focusing X-rays. The advantage of ELNES over XANES is the potential to examine small structural changes and variations in the local density of unoccupied electronic states at a nanometer level. As a trade-off of the high special resolution, one must pay attention to minimize the irradiation damage caused by focusing the electron beam on the ELNES measurements. X-ray beam, however, typically cannot be focused on the nano-sized area. ELNES can be measured with TEM. TEM was originally designed to observe the microstructure of a specimen through magnified image and to analyze the crystal structure through diffraction patterns.

Techniques to characterize the aromatic hydrocarbon species present are of interest with regard to the improved methods of recovery, as well understanding morphogenesis of these materials. Characteristic differences related to the degree of symmetry or the spatial arrangement of the fused ring aromatic hydrocarbons indicate that C 1*s* ELNES spectroscopy should be useful for characterizing aromatics in the bulk samples opaque to soft X-rays. It is important to understand the links between geometric/electronic structure and the observed spectra.

In the frame of core loss excitations, there is no comprehensive study on the ELNES spectra of the non-equivalent carbon atoms of phenanthrene and anthracene in the crystalline phases. In the aforementioned works, the fine spectral features have not been discussed in detail. The electronic structures of these two compounds are needed to be further investigated and compared. For these reasons, we have carried out a comparative study of distinct carbon atoms in the two isomer structures in the crystalline phases, including phenanthrene and anthracene, by means of inelastic electron scattering from the samples, ELNES analysis. Given that this comparison among core loss excitation is associated to distinct carbon atoms, the ELNES spectra calculated in this regard can be as an overture in the calculations of the organic crystal microscopy field. Therefore, the electronic properties of phenanthrene and a comparison with those of anthracene are essential, providing beneficial information for the future of their applications in electronics and materials science. We calculate the core loss spectra of distinct carbon atoms in crystalline

phenanthrene and anthracene by means of the FPLAPW method. This comparison reveals some interesting properties of their carbon-carbon bond lengths and chemical shifts. The paper is organized as follows. The next section gives an outline of the theoretical method and computational parameters used. Furthermore, we describe the structural properties of phenanthrene crystal in comparison to anthracene, and discuss the electronic band structures of two compounds. The focus is on the C K edge structures of phenanthrene with a comparison to anthracene.

2. Computational details

2.1. Calculation parameters

More computational parameters used here are the same as those in our previous work on the electronic and optical properties of phenanthrene and anthracene [18], i.e., electronic calculations done relativistically are based on the FPLAPW method. The exchange-correlation potential within the GGA has been calculated by means of Perdew, Burke and Ernzerhof (PBE) functional [31]. The muffin-tin radii in phenanthrene and anthracene have been fixed to 1.18 a.u. for carbon atoms (C) and to 0.6 a.u. for hydrogen atoms (H). A $R_{MT}K_{Max}$ equal 3.0 is sufficient to obtain reasonable ELNES spectra, and they have been chosen for phenanthrene and anthracene calculations as well. The G_{Max} parameter was taken to be 14 Bohr^{-1}. Brillouin zone (BZ) integrations within self-consistency cycles were performed via a tetrahedron method containing 27 and 14 k-points in the irreducible *BZ* of phenanthrene and anthracene structures, respectively, in order to calculate the C K edge spectra in super-cells including core-hole approximation. Some energy-dependent broadening with a linear Lorentzian function Γ=0.1E, originating from the excited states lifetime has been applied to obtain the smooth ELNES spectra.

Optimized atomic positions and structural properties used in this work were those of our previous study, which had been obtained based on numeric atom-centered orbitals (NAOs) method implemented in all-electron full potential electronic structure FHI-aims code [32], with the inclusion of dispersion interactions, Van der Waals (see tables I and II of ref. [18]).

2.2. ELNES method

We have calculated the core loss spectra of crystalline phenanthrene and anthracene and compared them. TELNES3 program [23] implemented in the WIEN2k calculates the ELNES spectrum in the LAPW basis set. Here, we have summarized the most important equations of the formalism:

Within the first Born approximation, the double differential scattering cross section (DDSCS) for inelastic electron scattering which involves the fully relativistic effects is given by [33, 34]:

$$\frac{\partial^2\sigma}{\partial\Omega\partial E}(E,\boldsymbol{q}) = \left[\frac{4\gamma^2}{a_0^2 q^4}\right]\frac{k_f}{k_i}\sum_{i,f}\left|\langle f|e^{i\vec{\boldsymbol{q}}.\vec{\boldsymbol{r}}}|i\rangle\right|^2 \delta\left(E-E_f+E_i\right), \quad (1)$$

where $\vec{q}=\vec{k}_i-\vec{k}_f$, a_0, E and $\gamma=\sqrt{1-\beta^2}$ are the momentum transfer, the Bohr radius, the energy loss and the relativistic factor, respectively. It can be written in a more traditional form, as:

$$\frac{\partial^2\sigma}{\partial\Omega\partial E}(E,\boldsymbol{q}) = \sum_{l_F}\left|M_{l_F}(E,\boldsymbol{q})\right|^2 \chi_{l_F}(E), \quad (2)$$

$\chi_{l_F}(E)$ is the local partial density of states at the energy E. The equation is a sum of transitions to the final states of l_F-character (s, p, d, …). M_{lF} ($\boldsymbol{q}$,E), is a smooth function of energy loss, representing the overall shape of the ionization edge, in a way that variations in DDSCS nearly represent the energy dependence of the densities of states (DOSs) above the Fermi level.

The core-hole left by the excited electron locally changes the potential. Therefore, the projected density of states is changed and the overall shape of the spectrum is strongly modified. The core-hole calculations have been carried out by reducing the occupancy of the core level corresponding to the observed edge. In order to avoid renormalization problems, the missing charge is added to the unit cell as a uniform background charge. We used 384 atoms (2×2×2) for phenanthrene and anthracene super-cell structures to avoid the interaction between the neighboring core-holes. These sizes of super-cells have been optimized up to the results of the spectra without changes.

3. Results and discussion

Figure. 1 represents the crystal structures of anthracene and phenanthrene. Phenanthrene (anthracene) unit cell contained two phenanthrene (anthracene) molecules placed in a herringbone arrangement in the *xy*-plane (shown in figure. 1) which were then stacked along *z*-direction and the long molecular axis was parallel to the long unit cell axis *c*. It was crystalized in a monoclinic structure with $P2_1$ ($P2_1/a$) symmetry. In the *xy*-plane, the two shorter inter-molecular C–C distances in phenanthrene (anthracene) were 3.49 (3.51) Å and 3.65 (3.98) Å along the length of phenanthrene (anthracene) molecule. The experimental correspondents of phenanthrene were 3.55 and 3.68 Å, respectively [35-36]. The typical intra-molecular nearest neighbor C–C distance in phenanthrene (anthracene) was 1.43 (1.42) Å, which was less than half the inter-molecular distance. The average nearest neighbor C–H in both phenanthrene and anthracene was 1.09 Å, similar to the experimental reports.

In our previous study, the calculated band structures and total densities of states (DOSs) of monoclinic phenanthrene and anthracene have been described in detail [18]; here, we deal with their band structures breifly. Our PBE-GGA results showed that phenanthrene and anthracene were semiconductors with direct band gaps 2.76 and 2.04 eV at Z point, respectively, in agreement with energy gap values and the overall dispersion of the bands with the previous theoretical studies [37-38]. Although there is not any study regarding the electronic band gap of phenanthrene in

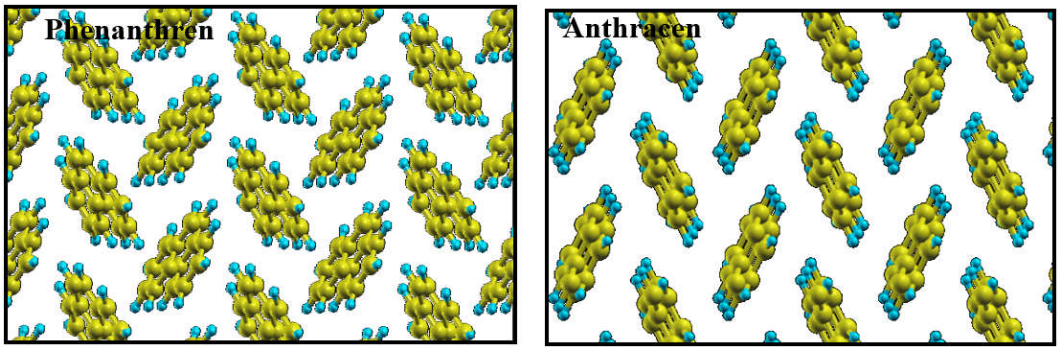

Figure 1. (color online) Crystal structures of phenanthrene (left) and anthracene (right) in the herringbone view (*xy*-plane). Large and small spheres are carbon and hydrogen atoms, respectively.

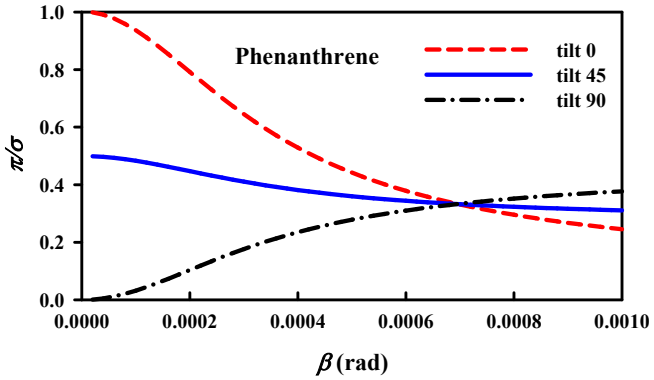

Figure. 2. (color online) The out-of-plane/in-plane (π/σ) ratio of carbon K edge in phenanthrene for a 300 keV beam and three sample-to-beam orientations (0, 45 and 90 degrees). The magic angle (0.69 mrad) occurs at the cross of the three curves.

photoemission experiments, the band gap of anthracene has been reported to be 3.7-4.4 eV [39-41]. However, the optical energy gap of phenanthrene (anthracene) has been reported to be 3.16 (3.11) eV [16]. The difference between experimental and computational energy gap was due to the approximation used for exchange-correlation functional in Kohn-Sham DFT. To correct the band gap values, within G_0W_0 approximation [42], we determined quasi-particle corrected gaps, i.e., the electronic gap of phenanthrene and anthracene. These QP gaps were 5.54 and 4.37 eV for phenanthrene and anthracene, respectively (figure 2 of ref. [18]).

By means of a 300 keV electron beam, we calculated the energy loss near the carbon K edge in phenanthrene and anthracene structures. The method for calculating ELNES used in the present work has been developed by Nelhiebel *et al.* [34]. As shown in figure 2, the simulated collection semi-angle has been set at the magic value of 0.69 mrad. This microscope setting was meant to obtain the orientation independent ELNES spectra. Since the ELNES measurements were sensitive to the relative orientation of sample and electron beam, and different orientations could lead to distinct ELNES spectra, we calculated collection semi-angle in the magic value in order to avoid this dependency. In fact, due to a well-defined orientation of the momentum transferred between the fast incoming electron and the target electron of the crystal with respect to the investigated crystalline sample, ELNES spectra were sensitive to anisotropy. For the identification of phases by fingerprints, one should, therefore, use experimental conditions in which the anisotropy effects are removed. The collection angle providing this condition is called the magic angle. Moreover, various approaches were used to calculate the spectra corresponding to the ground state and the full core-hole with different sizes of super-cells, Final State Rule, up to the convergence of the results.

Due to the selection of large size super-cells, in order to neglect the interaction between neighboring core-holes, due to the large energy gaps, ELNES spectra were very different in the ground state cells and super-cells, as can seen in figure 3. When a core-hole was created due to the excitation of a core electron, valence electrons moved, such that they could screen the core-hole potential. In metals, valence electrons could move easily, so the core-hole effect would be less significant, whereas in semiconductors, especially in insulators, the electrons could not move easily because of the filled valence band; therefore, the core-hole effect would contribute significantly to changing the unoccupied DOS. Since phenanthrene and anthracene semiconductors have rather large energy gaps, the screening effect on the core-hole by the valence electrons is weak. In our results, the immediate effect of the core-hole interaction in C K edges was the slight shifting of π^* edge to the lower energies and the drastic redistribution and displacement of σ^* intensity to the lower energies.

Figure 4 shows the computational C 1*s* ELNES spectra of phenanthrene and anthracene. A comparison between our ELNES spectra and the reported XANES calculations [30] indicated that while the main features

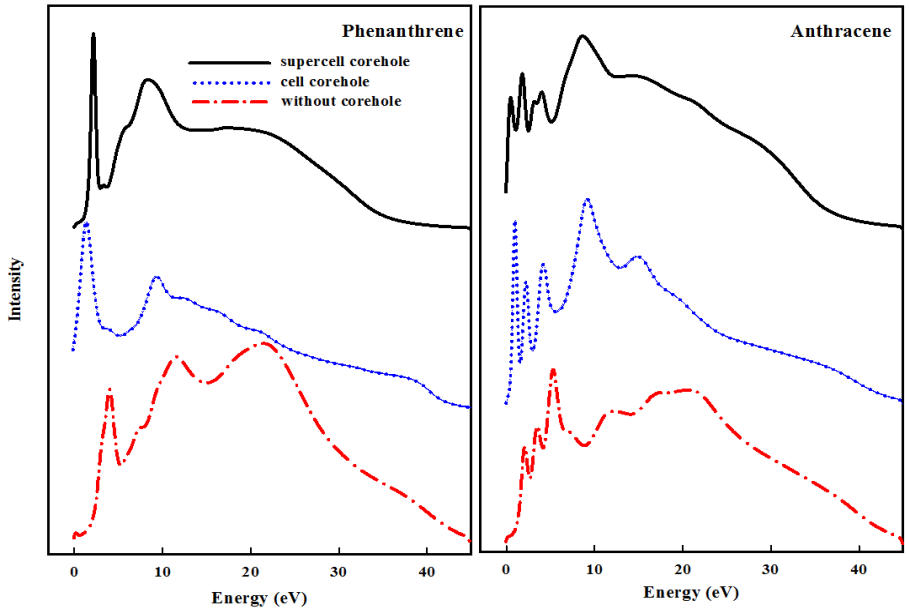

Figure 3. (color online) Super-cell size convergence of the calculated C K edge ELNES spectra of crystalline phenanthrene (left) and anthracene (right).

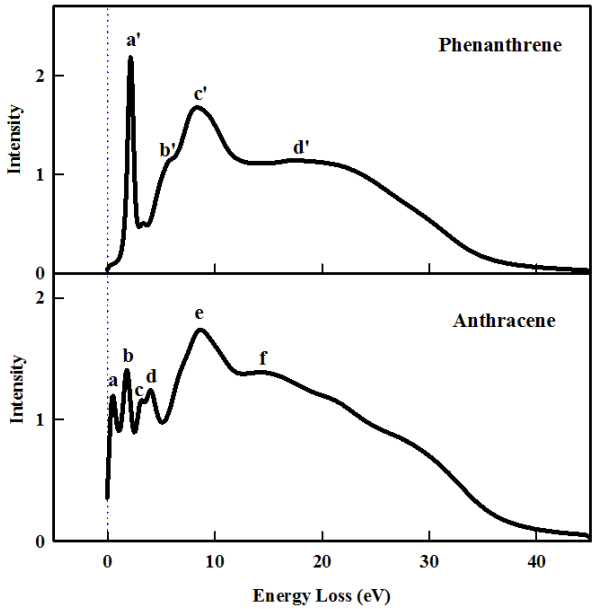

Figure 4. ELNES spectra of C K edges of crystalline phenanthrene (top) and anthracene (bottom).

for each species were observed at similar locations and with similar relative intensities, there were some differences between the results of the two techniques. One of the most striking ones was the absence of specific fine peaks, as well as reduced intensity or redistributed intensity at the edge onset of the reported XANES spectrum of phenanthrene [30].

Clearly, these two crystal structures showed highly different ELNES spectra, against on their structural similarities. The first main feature in the ELNES of phenanthrene, '*a*", occurred at 2.15 eV. It was accompanied by a broad shoulder, '*b*", at 5.7 eV, a rather broad peak, '*c*", at 8.35 eV, and a substantially broad peak, '*d*", at around 16.5 eV. Characteristic signatures of anthracene ELNES were two intense and sharp peaks, '*a*' and '*b*', at 0.5 eV and 1.8 eV, respectively, which were accompanied by the peaks with lower intensity at the higher energies, somewhat broader and partially overlapping peaks, '*c*' and '*d*', at 3.2 and 4.0 eV, a rather high intensity broad peak, '*e*', at 8.65 eV, and a substantially broader peak, 'f', around 14.3 eV. In addition to the much stronger splitting of the π^* peak into peaks '*a*' and '*b*' for anthracene, the splitting of σ^* peak into '*e*' and '*f*' was observable, whereas this was weak in phenanthrene. For the recognition of the origins of these features, we used two tools: the angular momentum projected local density of states (local DOS) and the spectral decomposition of the ELNES to its components. It is believed that ELNES probes the unoccupied local projected density of states of materials. The interpretation based on LDOS can be clearly seen in equation. (2). The energy dependence of the transition matrix elements is weak, meaning that C 1*s* ELNES is proportional to the unoccupied density of

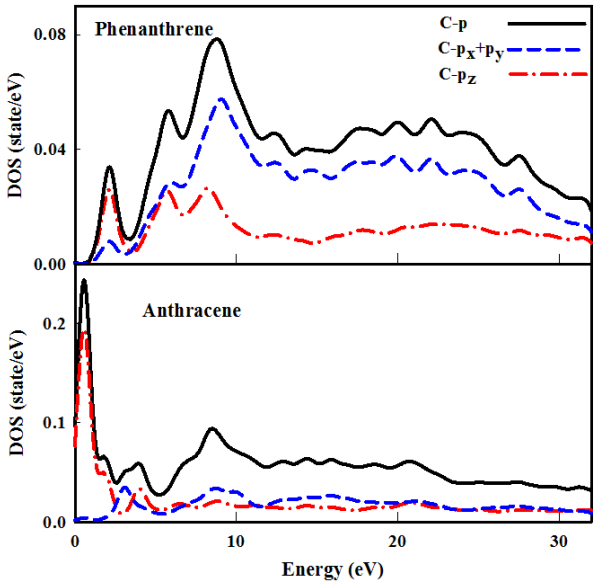

Figure 5. (color online) Partial density of states of carbon atom in crystalline phenanthrene (top) and anthracene (bottom).

states of C atom which is projected on *p*-momentum (according to the diploe selection rule, final states available for transition core electron are *p* states). In the second tool, ELNES is decomposed to its (l',m') components, by means of which the scattering is from an initial state $|nlm\rangle$ to the projection of final states onto the angular momentum state $|l',m'\rangle$.

A careful study of the local density of states in both structures revealed some interesting aspects. figure 5 represents the *p*-symmetry carbon DOS decomposed to π^* (p_z) and σ^* ($p_x \pm p_y$) components in phenanthrene and anthracene structures. Carbon *p*-LDOS of anthracene and its C K edge showed roughly similar dispersions. The first two peaks in the *p*-symmetry DOS of anthracene at about 0.5 and 1.8 eV originated from the purely π^* states (p_z), while other peaks at 3.18, 4.0 and 8.5 eV had almost equal contributions of π^* (p_z) and σ^* ($p_x \pm p_y$) states. Especially, the junction of peaks located at 3.14 and 4.0 eV clearly originated from the overlap of both π^* and σ^* components. It means that p_z electrons participated in the σ bonding for anthracene. Therefore, the first two peaks in anthracene ELNES could be attributed to the transition of carbon 1*s* to π^* states, and others to mostly σ^* states. It is confirmed by the ELNES decomposition to its components, π^* and σ^* contributions, as shown in figure 6. It reveals that the two sharp peaks at the edge onset of carbon K originated from only π^* states. At the end of these two sharp features (2.45 eV), the σ^* component overlapped with the π^*. It could be noticed that the broader and partially overlapping peaks, 'c' and 'd', at 3.2 and 4 eV, originated from both π^* and σ^* contributions. The former had more σ^* contribution, while the latter had more π^*. The origins of peak '*e*' and the broader one, '*f*', were both π^* and σ^* states. The onset of peak '*e*', at 7.4 eV, and the tail of the σ^* component, overlapped with the π^* spectrum. This was in agreement with the observation (see figure 5), showing that except the first two peaks, '*a*' and '*b*', in the overall *p*-LDOS spectrum of anthracene, there was a considerable DOS resulting from both π^* and σ^* orbitals.

Carbon *p*-LDOS of phenanthrene in the top of figure 5, like the carbon K edge, shows a peak at 2.12 eV, corresponding to the peak '*a*" in the phenanthrene ELNES, a broad peak at 5.8 eV corresponding to '*b*", which was accompanied by a higher intensity peak at the higher energy of 8.7 eV, corresponding to the '*c*" feature, and a broader one at around 17.0 eV, corresponding to '*d*" in carbon K edge of phenanthrene. Unlike anthracene, the first and third peaks had a considerable contribution of both π^* and σ^* states. The second one originated from more π^* orbitals and the other ones had contributions of both π^* and σ^* orbitals. This could be justified by means of phenanthrene ELNES decomposition in the top of figure 6. At around 6.2 eV, near the position of the broad peak '*b*',' the delocalized π-electrons participated in the σ bonding for the phenanthrene.

Some interesting aspects of organic molecular crystals can be clearly observed by comparing K edges of non-equivalent carbon atoms. figure 7 shows ELNES spectra for the four selective carbon atoms C_1 to C_4 in both crystalline phenanthrene and anthracene. In phenanthrene, C_3 and C_4 atoms were equivalent, while the four carbon atoms in anthracene were non-equivalent. The latter was as in the case of ref. [28], which was concerned with the NEXAFS spectra in a molecular anthracene. The Rydberg transitions in the K edges of four carbon atoms in the molecular anthracene, as observed in the NEXAFS spectra, have been reported by Klues *et al*. [28]; but they are not presented in the case of XANES or ELNES spectra of condensed anthracene. In addition, the absence, or possibly a shift to higher energies, in the spectra of anthracene in the solid phase, could be assigned to the Rydberg transitions in the gaseous species. It is clearly observable that C_i 1s ELNES spectra for the three non-equivalent carbon atoms (C_1, C_2 and C_3) in a phenanthrene molecule were egregiously different, whereas in anthracene, apart from

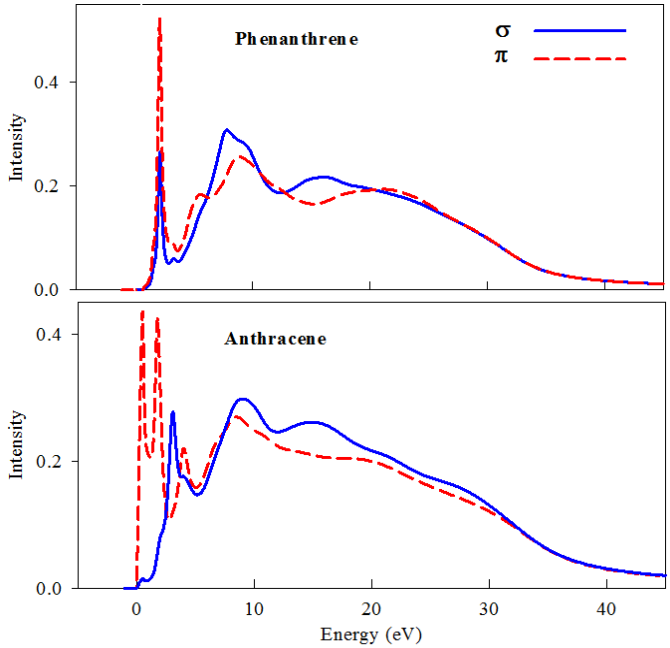

Figure 6. (color online) Spectral (l', m') decomposition of the ELNES spectra of crystalline phenanthrene (top) and anthracene (bottom). Total spectra are decomposed into the π^* (dashed lines) and σ^* (full lines) components. As a signature of π-σ hybridization in both structures, the σ^* component overlaps with the π^* spectrum at some energy position.

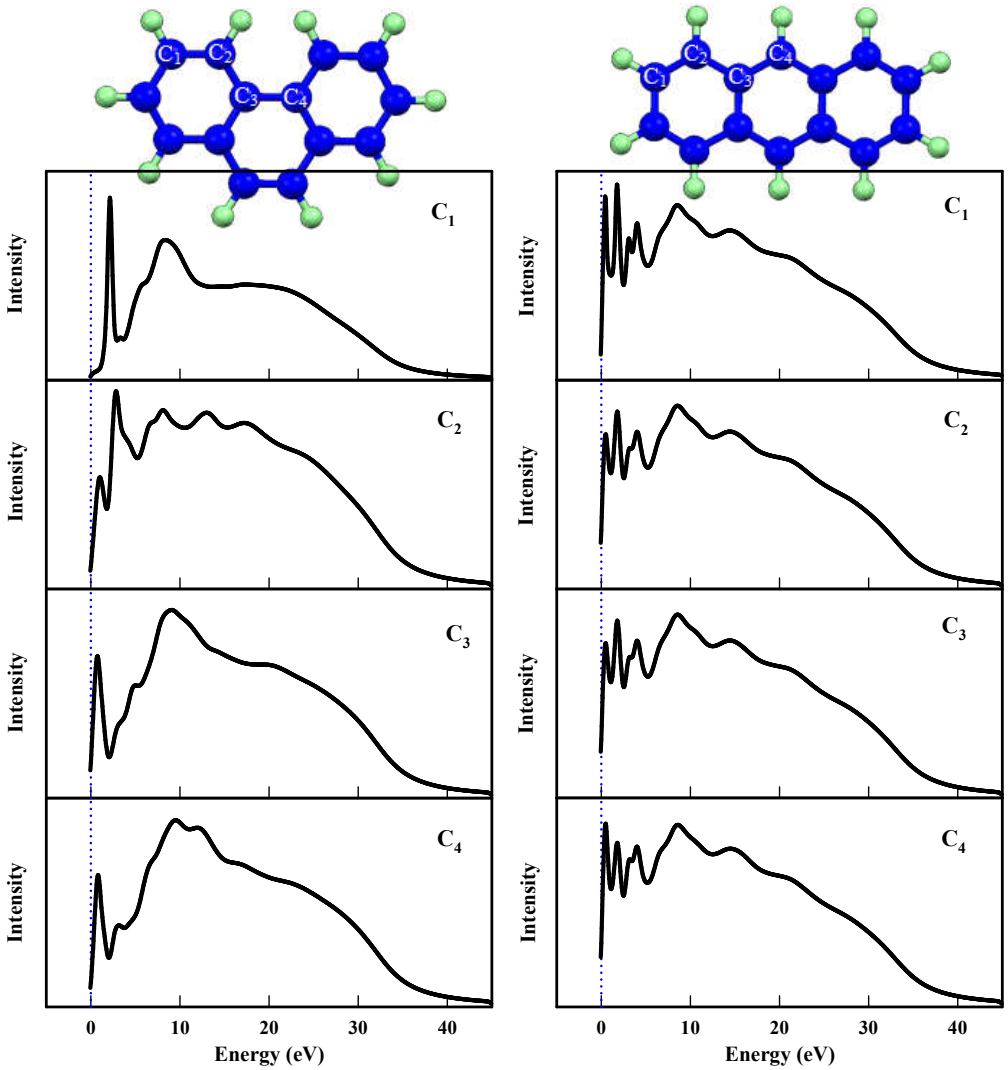

Figure 7. (color online) C K edges ELNES spectra in crystalline phenanthrene (left) and anthracene (right) for the four different carbon atoms represented in the top most figures.

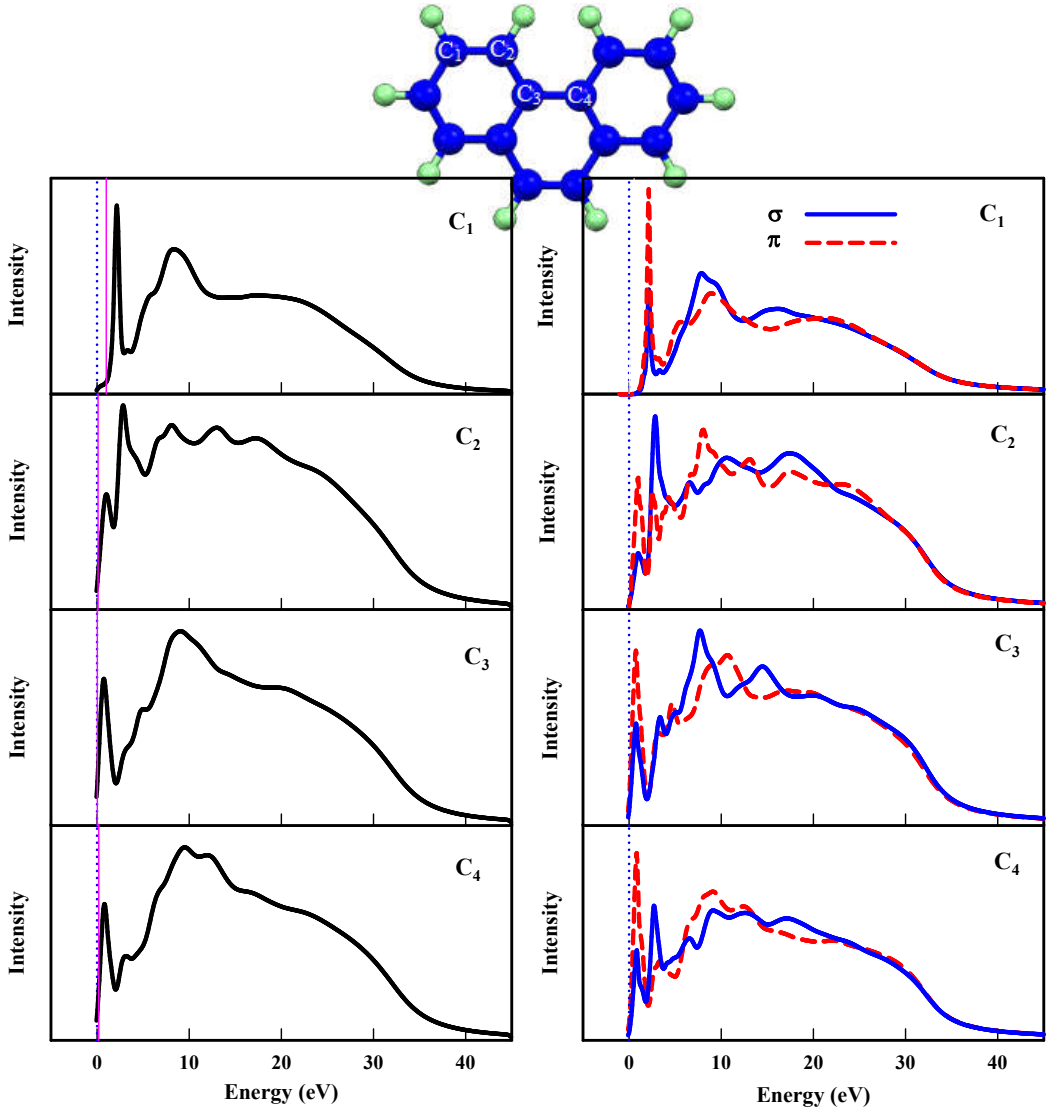

Figure 8. (color online) Left panels: calculated C 1*s* ELNES spectra of crystalline phenanthrene for the four different carbon atoms C_1 to C_4 , as represented in the top most figure. Right panels: C_1 to C_4 ELNES decomposition to π and σ components in phenanthrene.

a change in the relative intensity of the two two features of C_i K edges, there were no considerable changes. These behaviors could be due to the linear (angular) geometry of an anthracene (phenanthrene) molecule. In the case of equivalent carbon atoms, C_3 and C_4 in phenanthrene, the overall dispersions of the ELNES spectra were nearly the same. Some slight differences could be observed in the relative intensities and the presence of some fine structures. These differences could be attributed to the different C_2-C_3 and C_3-C_4 bond lengths. In organic molecular crystals, the C-C bond lengths and angles are well-known to be different in a single molecule. However, the C_1-C_2 bond length in phenanthrene was 1.383 Å, C_2-C_3 and C_3-C_4 are 1.410 and 1.431 Å, respectively. Therefore, the C-C bond lengths intensely impressed the fine structures in ELNES spectra. The distinct carbon K edge structures revealed the well-known sensitivity of the ELNES spectra to chemical bonding. In the spectra of Figure. 8, the vertical pink lines indicated the ionization thresholds of different carbon atoms in the crystalline phenanthrene, exhibiting only small variation, chemical shifts, 0.4 eV, between C_1 and three other carbons (see table I). The latter had negligible energy differences. It seemed that the smaller bond lengths pushed the ELNES features to the higher energies. In the right hand side of figure 8, the ELNES decomposition for these different symmetry non-equivalent carbon atoms has been displayed. It can be seen that the first peak in all ELNES spectra had the contributions of both π^* and σ^* structures. Moreover, C_2 to C_4 carbon atoms had partcularly various fine structures composed of both π and σ states.

Besides, the calculated ELNES features had counterparts in the projected DOS for both non-core-hole and core-hole calculations. figure 9 confirms this for both phenanthrene and anthracene structures. The calculated ELNES features in phenanthrene and anthracene were excellently reproduced by the projected DOS. There was an excellent agreement between *local* DOS and ELNES for the momentum resolved ELNES.

Table 1. Carbon 1*s* ionization edge (eV) for the four selective carbon atoms in crystalline phenanthrene.

Crystal	C_1	C_2	C_3	C_4
Phenanthrene	318.867	318.472	318.439	318.427

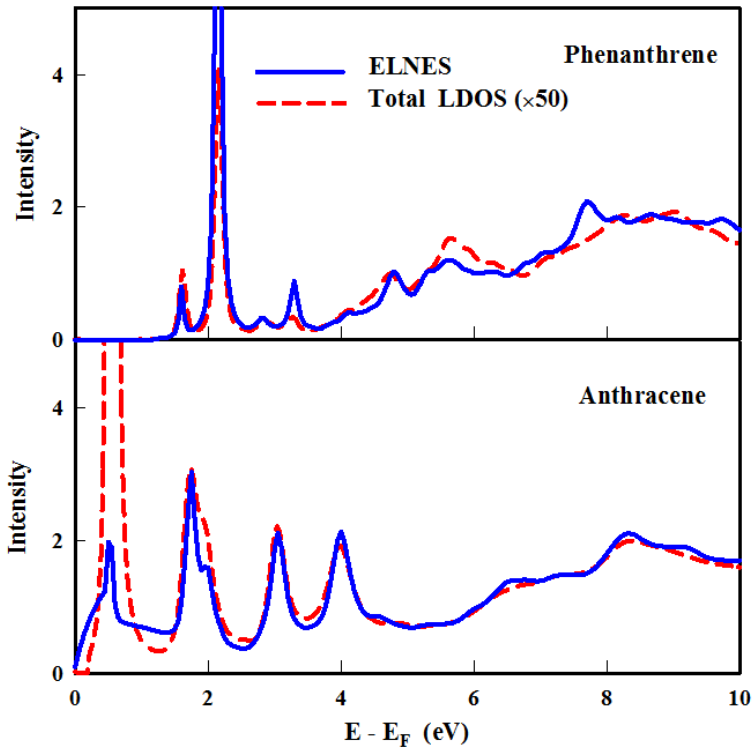

Figure 9. Local density of states (LDOS) of the carbon atom (dashed lines) in phenanthrene (top) and anthracene (bottom), as compared with the ELNES of the same atom with the core-hole included (solid lines).

This strong agreement between ELNES features and *local* DOS showed the weak energy dependence of the transition matrix elements, though these could be shown to depend strongly on the electron-beam orientation and the microscope settings. It also showed that the dipole selection rule governed the ELNES spectrum for phenanthrene and anthracene because all the ELNES features were those of the *p*-symmetry LDOS.

As mentioned above, ELNES spectra were different for two phases. It is well known that ELNES spectroscopy can be very useful to distinguish various local bonding structures in materials. The main differences between the ELNES spectra of phenanthrene and anthracene were: (i) the energy position of the edge-onset, which appeared at lower energies for anthracene due to its smaller computational band-gap; (ii) the much stronger splitting of π^* peak into a doublet peak in the edge-onset for anthracene; (iii) the high anisotropy in the K edge ELNES spectra of non-equivalent carbon atoms in phenanthrene in comparison with anthracene, which can be due to the angular geometry of a phenanthrene molecule; (iv) in addition, another difference in the ELNES spectra of phenanthrene and anthracene was the smaller energy difference between π and σ structures in phenanthrene, as compared to anthracene, due to the difference in the energy positions of the main σ^* states in the carbon K edge of phenanthrene and anthracene, '*c*'' in former and '*e*' in latter. This behavior showed the larger C–C bond length in phenanthrene in comparison to anthracene. It is well known that the size of C–C bond length strongly influences the ELNES spectrum [43], especially the σ^* edge-onset. Longer bonds tend to push the σ^* edge onset to the lower energies, in agreement with the lowering of the binding energies. Moreover, the smaller bond lengths display the ELNES features of distinct carbon edges at the higher energies.

4. Conclusions

The energy losses near the edge structures of two molecular crystals, namely, 'phenanthrene' and 'anthracene', were calculated in the framework of the density functional theory by means of the FPLAPW method. In the ELNES calculations, two approaches were used; they correspond to the ground state and the core-hole approximation. Because of the rather large band gaps, the inclusion of core-holes was found to be essential for the accurate reproduction of features in the ELNES spectra of phenanthrene and anthracene. The effects of the core-hole interaction were: the small shift of the π^* feature to the lower energies, and, simultaneously, the strong redistribution of the σ^* feature to the lower energy parts. We found that there were multiple features in the ELNES spectra of phenanthrene and anthracene that originated from the transition of C 1*s* electron to π^* and σ^* states.

The ELNES spectrum of phenanthrene included transition from 1s carbon orbital to π^* and σ^*, and the

shoulder originated from these two main features. In anthracene, the first two intense features had contributions of π^* orbitals, which were accompanied by some slight overlapping between π^* and σ^*. Moreover, in comparison to anthracene, the energy difference between π^* and σ^* features of C K edges in phenanthrene was decreased. The unoccupied DOSs of these molecular crystals introduced the above features amazingly, representing the weak energy dependence of the transition matrix elements and the strong dependence on the electron-beam orientation and the microscope settings. The correspondence between all ELNES features and the *p*-LDOS states indicated the ruling of the dipole selection rule on the ELNES spectra. Furthermore, C 1*s* ELNES of different-symmetry non-equivalent carbon atoms in phenanthrene and anthracene were calculated. Due to the high anisotropy originating from the angular geometry of a phenanthrene molecule, different carbon atoms display distinct ELNES spectra. This behavior could be related to the different carbon-carbon atoms. The small chemical shift in phenanthrene was observed, due to the slightly different ionization thresholds of non-equivalent carbon atoms.

Moreover, according to this prediction, ELNES could distinguish different types of molecular organic crystals with isomer structures. This was evidenced by finding the distinctive features in the ELNES spectra of the crystal structures of phenanthrene and anthracene.

References

1. C K Chiang, C R Fincher, Jr., Y W Park, A J Heeger, H Shirakawa, E J Louis, S C Gau, and A G MacDiarmid, *Phys. Rev. Lett*. **39** (1977) 1098.
2. A Kadyshevitch and R Naaman, *Phys. Rev. Lett*. **74** (1995) 3443.
3. E A Silinsh and V Capek, "*Organic Molecular Crystals*", AIP Press, New York (1994).
4. J D Wright, "*Molecular Crystals*", 2nd ed., Cambridge Univ. Press, UK (1995).
5. S R Forrest, *Nature* (London) **428** (2004) 911.
6. T W Kelly, P F Baude, Ch Gerlach, D E Ender, D Muyres, M A Hasse, D E Vogel, and S D Theiss, *Chem. Matter*. **16** (2004) 4413.
7. M Bendikov, F Wudl, and D F Perepichka, *Chem. Rev*. **104** (2004) 4891.
8. K Hummer and P Puschnig, C Ambrosch-Draxl, *Phys. Rev. Lett*. **92** (2004) 147402.
9. K Hummer, C. Ambrosch-Draxl, *Phys. Rev.* B **71** (2005) 081202.
10. K Hummer, C Ambrosch-Draxl, *Phys. Rev.* B **72** (2005) 205205.
11. S F Nelson, Y Y Lin, D J Gundlach, and T N Jackson, *Appl. Phys. Lett*. **72** (1998) 1854.
12. Y Kan, L Wang, H Yunchuan, W Guoshi, and Q Yong, *Appl. Phys. Lett*. **84** (2004) 1513.
13. I Shiyanovkaya, K D Singer, V Percec, T K Bera, Y Miura, and M Glodde, *Phys. Rev.* B **67** (2003) 035204.
14. M Oehzelt, R Resel, and A Nakayama, *Phys. Rev*. **66** (2002)174104.
15. K Hummer, P Puschnig, C Ambrosch-Draxl, *Physica Scripta*. T**109** (2004) 152.
16. M T Bhatti, M Ali, S G N., and M Saleh, *Turk. J. Phys*. **24** (2000) 673.
17. X F Wang, R H Liu, Z Gui, Y L Xie, Y J Yan, J J Ying, X G Luo, and X H Chen, *Nature. Commun*. **1115** (2011) 1.
18. M Dadsetani, H Nejatipour, and A Ebrahimian, *J. Phys. Chem. Solids* **80** (2015) 67.
19. M Dadsetani, A Ebrahimian, and H Nejatipour, *J. Materials Science in Semiconductor Processing*, in press.
20. R F Egerton, "*Electron Energy-Loss Spectroscopy in the Electron Microscope*", 2nd ed. Plenum (1996).
21. G A Botton, G Y Guo, W M Temmerman, and C J Humphreys, *Phys. Rev.* B **54** (1996) 1682.
22. T Mizoguchi, I Tanaka, S Yoshioka, M Kunisu, T Yamamoto, and W Y Ching, *Phys. Rev.* B **70** (2004) 045103.
23. P Blaha, K Schwarz, G Madsen, D Kvasicka, and J Luitz, "*WIEN2k, An Augmented Plane Wave + Local Orbital Program for Calculating Crystal Properties*", Technical Universitat, Wien, Austria (2001).
24. C Hébert, J Luitz, and P Schattschneider, *Micron* **34** (2003) 219.
25. J T Titantah and D Lamoen, *Phys. Rev.* B **70** (2004) 075115.
26. H Nejati and M Dadsetani, *Micron* **67** (2014) 30.
27. J Luitz, M Maier, C Hébert, P Schattschneider, P Blaha, K Schwarz, and B Jouffrey, *Eur. Phys. J.* B **21** (2001) 363.
28. M Klues, K Hermann, and G Witte, *J. Chem. Phys*. **140** (2014) 014302.
29. M L Gordon, D Tulumello, G Cooper, A P Hitchcock, P Glatzel, O C Mullins, S P Cramer, and U Bergmann, *J. Phys. Chem.* A **107** (2003) 8512.
30. A L Pitman, J A Mcleod, E K Sarbisheh, E Kurmaev, J Müller, and A Moewes, *J. Phys. Chem.* C **117** (2013) 19616.
31. J P Perdew, K Burke, and M Ernzerhof, *Phys. Rev. Lett*. **77** (1996) 3865.
32. V Blum, R Gehrke, F Hanke, P Havu, V Havu, X Ren, K Reuter, M Scheffler, *Computer Physics Communications* **180** (2009) 2175.
33. H A Bethe, *Ann. Phys*. **5** (1930) 325.
34. M Nelhiebel, P H Louf, P Schattschneider, P Blaha, K Schwarz, and B Jouffrey, *Phys. Rev.* B 59(1999) 12807.
35. D W Jones and J Yerkess, *J. Cryst. Mol. Struct*. **1** (1971) 17.
36. V C Sinclair, J Monteath Robertson, and A M Mathieson, *Acta Cryst*. **3** (1950) 251.
37. P L de Andres, A Guijarro, and J A Vergés, *Phys. Rev.* B **84** (2011) 144501.
38. K Hummer, P Puschnig, and C Ambrosch-Draxl, *Phys. Rev.* B **67** (2003) 184105.

39. G Vaubel and H Baessler, *Phys. Lett*. **27** (1968) 328.
40. E A Silinsh, "*Organic Molecular Crystals*", Springer-Verlag, Berlin, Heidelberg, New York (1980).
41. P J Bounds and W Siebrand, *Chem. Phys. Lett.* **75** (1980) 414.
42. L Hedin, *Phys. Rev*. **139** (1965) 796.
43. J T Titantah and D Lamoen, *Phys. Rev.* B **72** (2005) 193104.